JACS
JOURNAL OF THE AMERICAN CHEMICAL SOCIETY
Article
pubs.acs.org/JACS

Birch-Type Hydrogenation of Few-Layer Graphenes: Products and Mechanistic Implications

Xu Zhang,[†] Yuan Huang,[†] Shanshan Chen,[‡] Na Yeon Kim,[#] Wontaek Kim,[∥] David Schilter,[†] Mandakini Biswal,[†] Baowen Li,[†] Zonghoon Lee,[†,#] Sunmin Ryu,[∥,⊥] Christopher W. Bielawski,[†,§,□] Wolfgang S. Bacsa,[▽] and Rodney S. Ruoff[*,†,§,#]

[†]Center for Multidimensional Carbon Materials (CMCM), Institute for Basic Science (IBS), Ulsan 44919, Republic of Korea
[‡]Department of Physics, Renming University of China, Beijing 100782, P. R. China
[§]Department of Chemistry, Ulsan National Institute of Science and Technology (UNIST), Ulsan 44919, Republic of Korea
[∥]Department of Chemistry, Pohang University of Science and Technology (POSTECH), Pohang, Gyeongbuk 37673, Republic of Korea
[⊥]Division of Advanced Materials Science, POSTECH, Pohang, Gyeongbuk 37673, Republic of Korea
[#]School of Materials Science and Engineering, UNIST, Ulsan 44919, Republic of Korea
[▽]CEMES-CNRS and University of Toulouse, 29 rue Jeanne Marvig, 31055 Toulouse, France
[□]Department of Energy Engineering, UNIST, Ulsan 44919, Republic of Korea

Supporting Information

ABSTRACT: Few-layer graphenes, supported on Si with a superficial oxide layer, were subjected to a Birch-type reduction using Li and H_2O as the electron and proton donors, respectively. The extent of hydrogenation for bilayer graphene was estimated at 1.6−24.1% according to Raman and X-ray photoelectron spectroscopic data. While single-layer graphene reacts uniformly, few-layer graphenes were hydrogenated inward from the edges and/or defects. The role of these reactive sites was reflected in the inertness of pristine few-layer graphenes whose edges were sealed. Hydrogenation of labeled bilayer ($^{12}C/^{13}C$) and trilayer ($^{12}C/^{13}C/^{12}C$) graphenes afforded products whose sheets were hydrogenated to the same extent, implicating passage of reagents between the graphene layers and equal decoration of each graphene face. The reduction of few-layer graphenes introduces strain, allows tuning of optical transmission and fluorescence, and opens synthetic routes to long sought-after films containing sp^3-hybridized carbon.

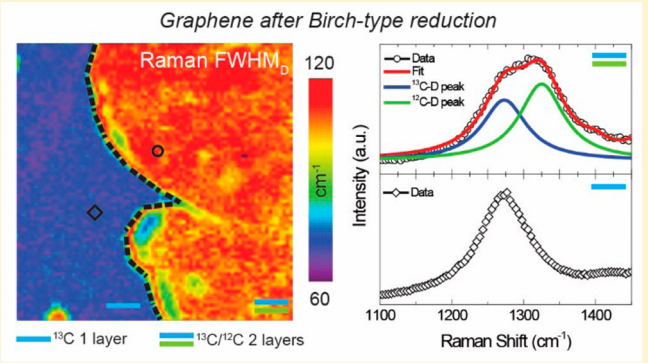

INTRODUCTION

The functionalization of graphene perturbs both its physical and chemical properties. Fully hydrogenated graphene, often referred to as graphane, is a wide band gap material according to theoretical calculations.[1,2] The removal of H atoms from one side of graphane affords graphone, a semihydrogenated graphene predicted to be a ferromagnet with an estimated Curie temperature of 278−417 K.[3] While stoichiometric graphane $(CH)_n$ and graphone $(CH_{0.5})_n$ have not, to the best of our knowledge, been prepared, the partial hydrogenation of graphene leads to "hydrogenated graphenes"[4] whose electronic band gap,[5−7] optical transmittance,[7] fluorescence,[8] and chemical reactivity[9] differ from that of the starting material. In this context, graphene hydrogenation is typically induced by exposure to hydrogen plasma[5−7,9−11] or by solution methods such as Birch-type reduction.[8,12−19]

In contrast to single-layer graphene (SLG), few-layer graphene (FLG, number of layers (n) ≥ 2) and bilayer graphene (BLG) in particular have nonzero band gaps as well as electronic structures that depend strongly on the stacking arrangement.[20] In terms of chemical reactivity, it is noted that BLG on SiO_2/Si is less prone to covalent functionalization relative to SLG on SiO_2/Si.[11,21] When considering the hydrogenation of SLG and BLG, the latter may afford a greater range of new materials, including one in which two graphane layers stack through van der Waals interactions.[22] A related material is H-terminated diamane,[23] which comprises two carbon sheets whose outer faces are hydrogenated. The inner faces are linked by C−C bonds between sp^3-hybridized C atoms in an arrangement reminiscent of diamond. Since such

Received: August 18, 2016
Published: November 2, 2016

DOI: 10.1021/jacs.6b08625
J. Am. Chem. Soc. 2016, 138, 14980−14986

two-dimensional materials typically sit atop a substrate, their individual layers are nonequivalent. Regardless, conversion to a diamane-like structure that features interlayer C−C bonds might be possible if, for example, the top face can undergo hydrogenation while the bottom bonds to a metal substrate.[24,25] A detailed study of FLG hydrogenation is necessary to delineate mechanistic and mass transport phenomena.

The Birch reduction involves the partial hydrogenation of aromatic molecules,[26] and although such a reaction is typically applied to small molecules, it has also been shown to be applicable to bulk carbon materials including graphite,[8,12−14] nanotubes,[12] and graphite oxide.[15,16] Recently, the scope of the reaction has been extended to include SLG on SiO_2/Si,[17,18] although detailed characterization of the products, including the final H atom coverage and distribution, has yet to be reported. The Birch-type reduction of atomically thin carbon materials is thus only lightly studied,[17,18] despite being necessary to understand the reactivity of carbon materials.

Aside from the fundamental value of investigating Birch-type reductions of carbon materials, the efficiency and scalability of the transformation make it potentially attractive for hydrogen storage.[16] The reaction gives rise to fluorescent graphitic materials,[8] and can also be used to finely tune electrical conductivity. For example, the Birch-type reduction of SiO_2/Si-supported SLG affords an insulator[17] which loses hydrogen at elevated temperatures. The dehydrogenated material exhibits electrical conductivity comparable to that of SLG, even though Raman spectroscopy indicated that the former contained a number of defects. Hydrogenated SLG bears a magnetization that has been studied using magnetic force microscopy, and the patterning of magnetic regions can be achieved using electron beam irradiation.[18]

Despite the attractive properties of hydrogenated graphenes, the mechanism by which SLG undergoes Birch-type hydrogenation has yet to be thoroughly explored. We not only address this deficiency, but also extend the methodology to the more challenging precursors, including BLG and trilayer graphene (TLG). The hydrogenation of FLGs may involve several processes such as diffusion of reagents at edges and defects, as well as mechanisms in which the supporting SiO_2 plays a role. The reactivities of FLGs are readily studied using Raman spectroscopy, which we apply to multilayered graphenes prepared from natural abundance as well as isotopically enriched sources of carbon (e.g., $^{13}C/^{12}C$ BLG and $^{12}C/^{13}C/^{12}C$ TLG). To gain additional insight into the hydrogenation mechanism, FLG samples with sealed edges were also examined. By monitoring the regiochemical outcomes of these reactions, a deeper understanding of Birch-type reductions of graphenes is obtained and described below. Also presented is a comparison of the structural characteristics and optical properties displayed by the starting materials and their reduced products.

RESULTS AND DISCUSSION

Wet-Chemical Hydrogenation and Thermal Dehydrogenation. A graphene flake containing SLG and AB-stacked BLG (AB-BLG) regions was prepared by mechanical exfoliation onto SiO_2 (300 nm)/Si. Atomic force microscope (AFM) images of the material revealed two regions whose darker and lighter contrast are attributed to SLG and BLG, respectively (Figure 1a). While the regions are discernible in terms of their height profiles (see Figure S1a), the number of layers and stacking order in few-layer graphene (FLG) is also clear from

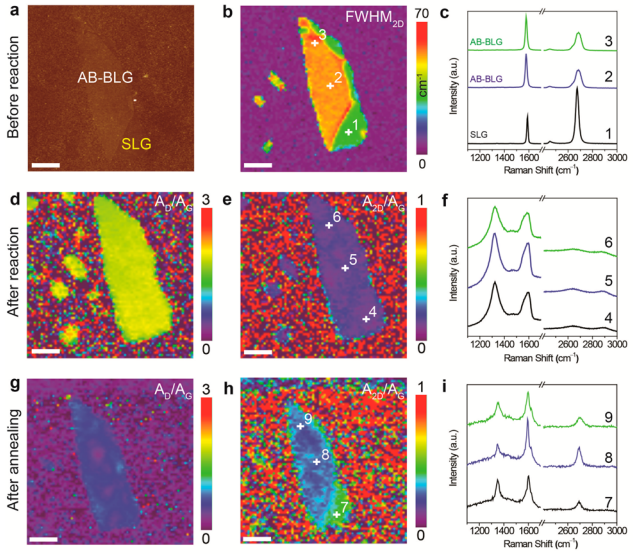

Figure 1. Mechanically exfoliated BLG before and after exposure to Birch-type reduction conditions as well as after annealing. (a) AFM topography image and (b) Raman map of the 2D peak width ($FWHM_{2D}$) for pristine graphene. (c) Raman spectra acquired at the SLG and AB-BLG positions marked in b. (d) Raman map of the intensity (area) ratio of the D and G bands (A_D/A_G) and (e) Raman map of the intensity (area) ratio of the 2D and G bands (A_{2D}/A_G) after reduction in solution of Li in liquid NH_3 for 10 min. (f) Raman spectra acquired at the positions marked in part e. (g) Raman map of the A_D/A_G ratio and (h) Raman map of the A_{2D}/A_G ratio after annealing at 700 °C in Ar for 3 h. (i) Raman spectra obtained at positions marked in part h. The scale bars are 3 μm.

Raman spectroscopic analysis.[27] The SLG regions give rise to sharp 2D bands, with uniform full width at half-maximum ($FWHM_{2D}$) values of 30 cm^{-1}. The 2D bands of the AB-BLG regions are uniformly broader (~55 cm^{-1}, Figure 1b). The D band, characteristic of defects and edge states, is absent for both SLG and AB-BLG. These apparently pristine materials (SI, Figure S2b) were subjected to Raman analysis, and full spectra at the three positions marked in Figure 1b are consistent with the assignment of SLG and AB-BLG regions (Figure 1c).

Birch-type reactions were performed by immersing SiO_2/Si-supported graphenes into Li/NH_3 solutions for 10 min to facilitate reduction. In a subsequent protonation step, the resulting reduced sheets, termed graphenides, were quenched by the addition of H_2O as the H^+ donor, a reaction signaled by a disappearance of the blue color characteristic of Li/NH_3 mixtures (see Experimental Section). The structures of SLG and AB-BLG are significantly altered by the Birch-type reduction, with the products exhibiting uniformly high Raman A_D/A_G values (~2) over the entire flake (Figure 1d). Modes giving rise to the D band can be populated upon introduction of sp^3-hybridized C centers in the form of C−H as well as C−O/N groups, the latter arising from side reactions (as determined using X-ray photoelectron spectroscopy (XPS), SI, Figure S3). Such sp^3-C sites break the translational symmetry of the hexagonal lattice,[28] and hydrogenated SLG and BLG, denoted here as H-SLG and H-BLG, respectively, thus give rise to weaker 2D bands and lower A_{2D}/A_G values (Figure 1e). The Raman spectra acquired at the three positions marked in Figure 1e all feature a strong and broad D peak at 1322 cm^{-1}, a broad G peak at 1595 cm^{-1} (merged with the D′ peak), a less intense 2D peak at ~2650 cm^{-1}, and a new weaker

DOI: 10.1021/jacs.6b08625
J. Am. Chem. Soc. 2016, 138, 14980−14986

D + G band at ~2890 cm^{-1} (Figure 1f).[28] The data indicate that the Birch-type reaction conditions induce extensive functionalization of SLG and AB-BLG within the 10 min reduction time.

The extent of hydrogenation was estimated by a detailed analysis of the Raman bands, although it is noted that this method likely affords lower bounds (see below). Raman spectroscopy enables one to conveniently quantify the defect density in graphene,[29−31] with diagnostic Raman parameters (i.e., A_D/A_G and A_{2D}/A_G ratios, 2D band energies, and D and 2D peak widths) for materials described here being compared to those recorded for SLG/BLG materials whose defects are induced by ion bombardment.[29−31] Our measurements indicate that each of the hydrogenated materials is a "stage II" graphene,[29−31] in which the average defect distance (L_D) is 1.5 ± 0.3 nm. In this context, the "defects" are assigned as sp^3-hybridized C atoms bonded to H, although the presence of trace amounts of C−O and/or C−N groups cannot be ruled out. In this case, 1.6 ± 0.6% of the C atoms are functionalized, a value that corresponds to a defect density of 6.3 ± 2.5 × 10^{13} cm^{-2}. Such sp^3-hybridized C atoms are known to give rise to D modes within an "activated region" of radius ~3 nm,[31] a value considerably larger than L_D. Thus, each "activated region" will on average contain more than one sp^3-hybridized C site,[31] and the density of these sites, as determined from L_D, will represent a lower limit. For comparison, when hydrogen coverages were estimated using XPS (C 1s peak deconvolution), the values for H-SLG and H-BLG were calculated to be 30.5 ± 1.5% and 24.1 ± 2.1%, respectively (SI, Figure S3).

The thermal stabilities of the hydrogenated graphenes were probed by heating samples under Ar (1.5 × 10^{-1} Torr), first at 300 °C, then 500 °C, and finally 700 °C (SI, Figure S4). Raman analysis of the annealed samples indicates that H-BLG has a higher thermal stability than H-SLG. After annealing at 700 °C, the A_D/A_G ratios of H-SLG and H-BLG in the Raman map decrease significantly (Figure 1g), while the A_{2D}/A_G ratios show the opposite trend (Figure 1h), a result consistent with dehydrogenation to the respective SLG and BLG starting materials. The Raman bands (Figure 1i) acquired at multiple positions (Figure 1h) narrow upon annealing of H-SLG and H-BLG, while the 2D peaks hypsochromically shift to 2692 and 2700 cm^{-1}, respectively. The latter result may be due to doping induced by exposure to H_2O and O_2 in the atmosphere.[32−34] Aside from thermal annealing, laser irradiation also appears to be a rapid and efficient means to convert H-SLG or H-BLG to their respective starting materials (Figure S5).

Elucidation of the Hydrogenation Mechanism. The hydrogenations of SLG and FLG were monitored by Raman spectroscopy, and it was found that each sample followed different reaction pathways. SLG on either SiO_2/Si or h-BN/SiO_2/Si can be hydrogenated uniformly by treatment with a solution of Li in NH_3 for 2 min, followed by subsequent exposure to H_2O (SI, Figure S6). The hydrogenation appears to be even and rapid, which suggests to us that the reaction occurs at comparable rates across the carbon material. While no D band was observed in the Raman spectra recorded for AB-BLG on SiO_2/Si (Figure 2a and Figure S7), a band emerged at the perimeter after exposure of the material to the reaction conditions described above (Figure 2b). The edges give rise to A_D/A_G ratios that are high (~1.8) when compared to those of the interior (~0.3). When subjected to Li/NH_3 for a further 8 min, the sample flake afforded uniform A_D/A_G ratios (Figure 2c). Thus, while the final product is uniform, the reaction

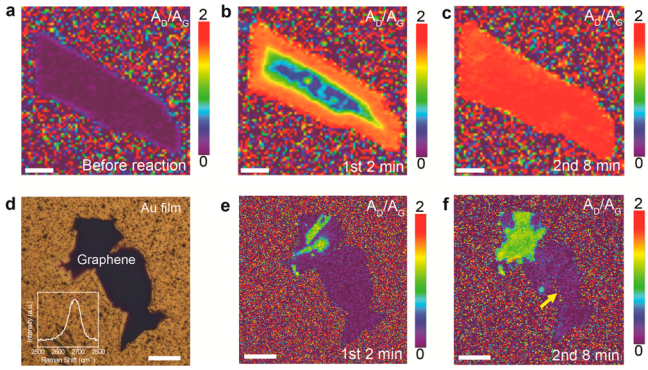

Figure 2. Structural evolution of BLG and edge-covered FLG during a Birch-type reduction. (a−c) Evolution of the Raman A_D/A_G map for AB-BLG during Birch-type reduction (a) before reduction, (b) after exposure for 2 min to a solution of Li in liquid NH_3, and (c) after further exposure for 8 min. (d) Optical image of the edge-covered FLG. The FLG 2D peak is shown as inset image. (e, f) Raman A_D/A_G map of the edge-covered FLG (e) after exposure for 2 min to a solution of Li in liquid NH_3 and (f) after further exposure for 8 min. The scale bars in parts a−c and d−f are 3 and 20 μm, respectively.

appears to proceed preferentially from the perimeter to the interior.

The role that edges play in the reaction mechanism was probed by sealing the perimeter of a FLG sample with an inert gold film before subjecting it to the hydrogenation conditions (Figure 2d and SI, Figure S8). Analysis of the Raman 2D band for the sealed FLG indicated it to be a pristine material containing more than three layers (Figure 2d). The sealed FLG is largely unaffected by exposure to the Li/NH_3 solution for 2 min (Figure 2e) followed by quenching with H_2O; no D peaks are observed at the FLG/gold boundaries, which apparently remain pristine. This observation implies that the Birch-type hydrogenation of FLG does not proceed unless defects or edges are exposed. Indeed, the only region of the sealed sample to be hydrogenated was an interior region that had likely been damaged during the sealing or hydrogenation step. When the sample was returned to the Li/NH_3 solution for an additional 8 min, the hydrogenation proceeded further from the damaged regions (Figure 2f). Although a torn region was found after the second hydrogenation step (see arrows in SI, Figure S9), the FLG/gold boundaries appeared to remain pristine.

In general, the Birch-type reduction of graphene requires two steps: (i) addition of alkali metal in liquid NH_3 to reduce the carbon and (ii) addition of a H^+ donor to complete the hydrogenation. In the first step, solvated electrons from the alkali metal are thought to reduce the graphene to the corresponding graphenide. Other reductants that afford similar outcomes, such as KC_8, are known, and their formation involves the intercalation of an alkali metal into the carbon matrix. Likewise, intercalation appears to be involved in the reduction of FLG and may initiate at edges and defects. Hydrolysis of the graphenide may then result in the formation of C−H bonds, with the conversion ceasing once the characteristic blue color of the Li/NH_3 solution disappears (~2 min). Indeed, leaving BLG exposed to media that contain H_2O for durations up to 60 min affords samples whose Raman data are virtually identical to those treated as described above (Figure 1).

The efficiency of the Birch-type graphene hydrogenation depends on the H^+ donor, and CH_3OH, despite being a widely

DOI: 10.1021/jacs.6b08625
J. Am. Chem. Soc. 2016, 138, 14980−14986

used H^+ donor in such reactions, is less efficient than H_2O for hydrogenating mechanically exfoliated FLG (SI, Figures S10 and S11). A less important factor in the reaction is the mode of interlayer stacking, and differently orientated CVD-grown BLG and TLG regions afford similar results (SI, Figures S12 and S13).

Hydrogenation of Isotopically Labeled BLG and TLG. Additional insight into the Birch-type reductions of FLGs was gained by studying isotopically labeled BLG and TLG. The enriched BLG material features a layer of ^{13}C atoms and another layer of carbon atoms in their natural abundance (98.9% ^{12}C). Such materials were prepared using the CVD pocket method[35,36] and feature sheets that are spectroscopically distinguishable, as the greater mass of ^{13}C relative to ^{12}C results in the former giving rise to lower energy Raman G bands (ω_{13G} = 1523 cm^{-1}) than the latter (when ω_{12G} = 1585 cm^{-1}).[37−39] The labeled BLG was characterized by Raman spectroscopy, and a map of the intensity (area) ratio of ^{12}C and ^{13}C G bands (A_{12G}/A_{13G}) is presented in Figure 3a. While the left region

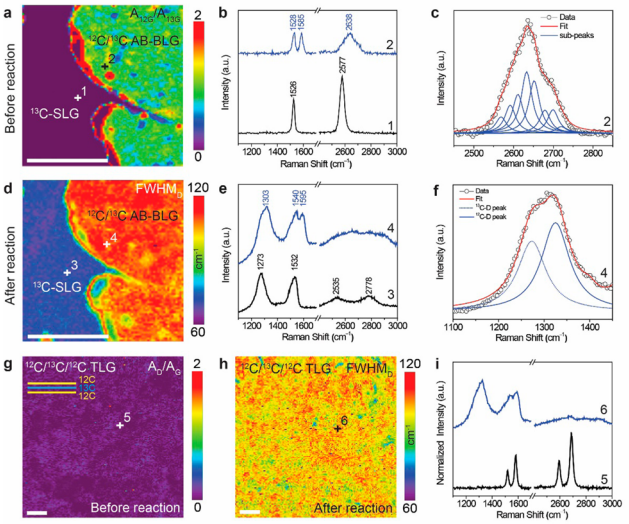

Figure 3. Raman maps of isotopically labeled graphene on SiO_2/Si. (a) A_{12G}/A_{13G} map of a selected region covered by SLG and BLG. (b) Raman spectra obtained at the positions marked in part a. (c) Fitting of 2D peak for $^{12}C/^{13}C$ BLG. (d) $FWHM_D$ map of the same region in part a after Birch-type reduction. (e) Raman spectra obtained at the positions marked in part d. (f) Fitting of D peak for $^{12}C/^{13}C$ BLG after hydrogenation. (g) A_D/A_G map of sequentially transferred $^{12}C/^{13}C/^{12}C$ TLG before hydrogenation. (h) $FWHM_D$ map of the same region in part g after Birch-type reduction. (i) Raman spectra obtained at the positions marked in parts g and h. The scale bars are 10 μm.

only features bands arising from ^{13}C SLG (Figure 3b), the right region has both ^{12}C- and ^{13}C-derived G bands. The similar intensities of these bands are consistent with an isotope ratio of ~1:1. The bilayer gives rise to resolvable ^{12}C and ^{13}C Raman G bands, but only a single broad 2D peak (2638 cm^{-1}, Figure 3b).[39] The overlap of phonons of the AB-stacked ^{12}C and ^{13}C layers results in the 2D peak not being split, although it can be fitted with eight Lorentzians (Figure 3c).[39] The absence of a D band in both the SLG (^{13}C) and BLG (^{13}C and ^{12}C) regions indicates that the graphene layers are of high quality (Figure S14b).

The labeled BLG was exposed to a solution of Li/NH_3 for 10 min before being quenched with H_2O, after which the region shown in Figure 3a gave rise to intense D peaks. Upon hydrogenation, the D peaks recorded for ^{13}C and ^{12}C BLG are broader than those observed for ^{13}C SLG (Figure 3d). Raman data for the ^{13}C SLG region (Figure 3e) features bands similar to those for hydrogenated graphene, albeit bathochromically shifted. In contrast, hydrogenated BLG gives rise to a broader D band at 1303 cm^{-1}, as well as two G peaks and a relatively broad feature between 2400 and 3000 cm^{-1}. The D peak was fitted with Lorentzians centered at 1325 and 1273 cm^{-1}, which corresponded to the ^{12}C and ^{13}C D bands, respectively (Figure 3f). The bands are similarly intense, implying that the ^{12}C and ^{13}C BLG layers are hydrogenated to the same extent.

A labeled TLG was studied to help determine if hydrogenation of the bottom layer requires intercalation of reagents between graphene layers or between the SiO_2/graphene junction, as well as to ascertain which faces are hydrogenated. The material was prepared by sequentially transferring ^{12}C, ^{13}C, and ^{12}C sheets onto SiO_2/Si. The TLG used was of high crystallinity, with the low defect density apparent from the low D band intensities A_D (and, hence, A_D/A_G) across the surface (Figure 3g and SI, Figure S15). After exposure of the material to the reduction conditions described above, a D peak appears over the entire TLG region studied ($FWHM_D$ ~100 cm^{-1}, Figure 3h), a result consistent with a reaction occurring at all of the layers (Figure 3i). Fitting the D peaks with Lorentzians revealed contributions from ^{12}C and ^{13}C D bands centered at 1325 and 1273 cm^{-1}, respectively (SI, Figure S15g−i). The hydrogenation of the middle ^{13}C layer suggests to us that intercalation of reagents between the graphene layers must play a role in hydrogenation. Since both faces of the ^{13}C layer are covered by graphene, the extent of hydrogenation is likely to be similar on both faces of the middle layer. The reactivity of individual graphene faces is rarely considered, and the present data indicate that each face in TLG is comparably reactive. If this were not to be the case, one would expect the layers to be hydrogenated to different extents. Although it is unclear how, or even if, the SiO_2 layer influences TLG reactivity, the similar reactivity of the individual layers indicates that any substrate effects are similar in nature for each layer. It is also not known how the lower layers accept protons, although graphene's permeability may be important in this regard.[40] A possible reaction sequence may first involve Li intercalation to give the corresponding Li graphenides. Then, H_2O could deliver H^+ either at the edges or to the topmost graphene face, through which H^+ might tunnel and be relayed to lower layers.

Hydrogenation-Induced Surface Strain/Deformation. The Birch-type reduction of FLGs not only influences the intensities of the material's Raman bands but also their energies. Spectra recorded for graphenes exposed to the hydrogenation conditions feature D, G, and 2D bands at energies that are ~20, 19, and 39 cm^{-1} lower than those for graphene reduced by hydrogen plasma (Figure 4a).[28] The spectral shifts for the reduced graphenes are independent of the substrate (SiO_2/Si, h-BN, Cu, Ni or Cu/Ni alloy (90/10)), the number of layers, and the H^+ donor source (H_2O, CH_3OH, or CH_3CH_2OH). In general, graphene band energies are sensitive to any physical or chemical perturbation. For example, when pristine graphene is subjected to mechanical strain, a shift ratio of $\Delta\omega_{2D}/\Delta\omega_G$ = 2.2 ± 0.2 is observed;[34,39] in comparison, the use of defect-rich graphene was reported to result in a shift ratio of $\Delta\omega_{2D}/\Delta\omega_D$ = 2.05.[41] Compared to the effects of strain, spectral changes resulting from hole doping ($\Delta\omega_{2D}/\Delta\omega_G$ = 0.75 ± 0.04) or electron doping ($\Delta\omega_{2D}/\Delta\omega_G$ < 0.75) are

DOI: 10.1021/jacs.6b08625
J. Am. Chem. Soc. 2016, 138, 14980−14986

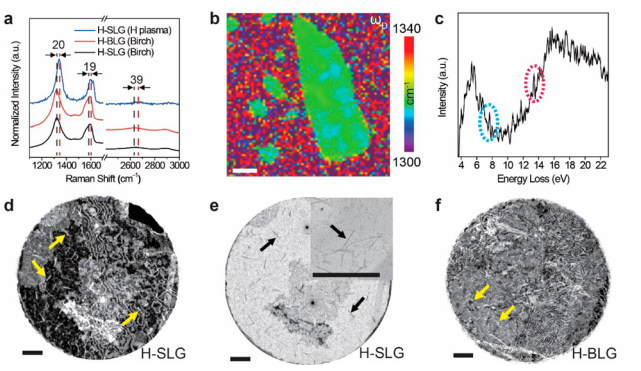

Figure 4. Structural deformation of hydrogenated graphene. (a) Raman spectra of SLG after hydrogenation by either Birch-type reduction or exposure to hydrogen plasma. (b) Raman map of D band frequency (ω_D) of the hydrogenated SLG flake shown in Figure 1a. The scale bar is 3 μm. (c) EELS of hydrogenated CVD-grown SLG after Birch-type reduction. (d) TEM dark-field image and (e) bright-field image of SLG after Birch-type reduction. The inset shows a higher magnification. (f) TEM dark-field image of BLG after Birch-type reduction. The scale bars in parts d–f are 300 nm.

relatively small.[34] When graphene undergoes covalent functionalization (e.g., using diazonium chemistry), $\Delta\omega_{2D}/\Delta\omega_G$ falls in the range 1.0–5.5 and is nonlinear with the extent of reaction because ω_G is sensitive to the presence of defects and structures that give rise to a D′ band.[42] These values indicate that strain can not only be effected mechanically, but also chemically, as the introduction of sp^3-hybridized C sites give rise to a D band ($\Delta\omega_{2D}/\Delta\omega_D$ = 1.8 ± 0.2).[42] As mentioned above, the data recorded for H-SLG, H-BLG, and H-TLG afforded similar ratios ($\Delta\omega_{2D}/\Delta\omega_G$ = 39/19 = 2.1, $\Delta\omega_{2D}/\Delta\omega_D$ = 39/20 = 2.0) consistent with the introduction of strain (Figure 4b). Indeed, the bathochromic shifts observed for the D, G, and 2D bands are greater than those obtained by doping (described above) or by Ar^+ ion bombardment,[29] underscoring the strained nature of the H-SLG and H-BLG materials prepared here.[34,41–43]

The presence of strain in H-SLG and H-BLG is to be expected as the newly formed sp^3-hybridized C sites would have elongated C–C bonds, although the resulting compression of the surrounding region may be attenuated by the sp^3-hybridized C atoms shifting from the basal plane. The formation of sp^3-hybridized C sites was investigated by transmission electron microscopy (TEM), using H-SLG and H-BLG obtained by the Birch-type reduction of CVD-grown SLG and BLG, each atop a TEM grid (Au Quantifoil). Signals were observed at 13.4 and 7.6 eV in the electron energy loss spectrum (EELS, Figure 4c) recorded for H-SLG. The former signal is assigned to the ground state excitation of bonded hydrogen,[44] whereas the latter is similar in energy to that reported for unpassivated diamond surfaces, in which transformation of dangling bonds into π-bonded chains induces partial graphitization.[44] These results, combined with the observations of a π-plasmon at ~5 eV, suggested to us that some of the carbon atoms present in the product were not bonded to at least one hydrogen atom. Moreover, the hydrogenation methodology appears to induce structural deformation,[45] as dark- and bright-field TEM analyses reveal wrinkles in H-SLG (marked by arrows in Figure 4d,e), whose structure contrasts the flat morphology of SLG (SI, Figure S16a–d). Similarly wrinkled structures are present in H-BLG (Figure 4f and SI, Figure S16e), and are consistent with the roughness of hydrogenated SLG/BLG on SiO_2/Si, as determined using AFM (SI, Figure S1b).

Optical Spectroscopy of Hydrogenated Graphene. The effects of hydrogenation on the optical and electronic properties of graphenes were studied using UV–vis spectroscopy. On quartz, both H-SLG and H-BLG derived from CVD-grown graphenes featured a broad absorption at 267 nm (Figure 5a), whose corresponding energy (4.64 eV) is close to

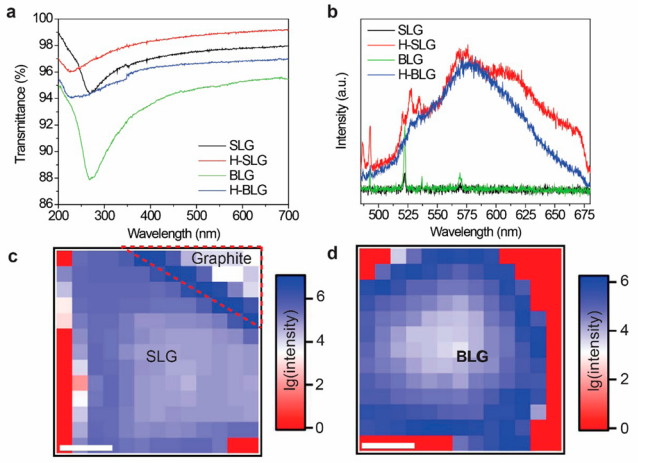

Figure 5. UV–vis transmittance spectra and fluorescence map of hydrogenated graphene. (a) UV–vis transmittance spectra of CVD-grown SLG and BLG on quartz before and after hydrogenation. (b) Fluorescence spectra of mechanically exfoliated SLG and BLG on SiO_2/Si before and after hydrogenation. (c) Fluorescence map of hydrogenated SLG (with graphite flake). (d) Fluorescence map of hydrogenated BLG. In parts c and d, the fluorescence intensity is integrated over 485–680 nm, and shown as the logarithm to base 10. The scale bars in parts c and d are 3 μm.

the π-plasmon energy of graphene.[7] The transparencies of SLG and BLG at 550 nm are 97.7% and 95.0%, respectively, with the optical absorbance for SLG (2.3%) being consistent with a value reported in the literature.[46] After hydrogenation, the absorptions shift from 267 to 226 nm (5.49 eV), with H-SLG and H-BLG becoming more transparent at 550 nm (98.9% and 96.8%, respectively), consistent with an opening of a band gap. The optical absorbance of H-BLG (3.2%) is more than double that of H-SLG (1.1%), a result that, along with the XPS data, indicates that the Birch-type reduction is less effective for BLG than for SLG.

The fluorescence of graphenes subjected to Birch-type reductions was also investigated (Figure 5b–d). Emission spectra of mechanically exfoliated SLG and BLG (SI, Figure S17, λ_{ex} = 457 nm), as well as those for H-SLG and H-BLG, are presented in Figure 5b. While neither pristine SLG nor BLG exhibit noticeable fluorescence, strong and broad emission bands for H-SLG and H-BLG were observed.[8,14] The fluorescence of graphite oxide has been attributed to nanographene domains surrounded by functionalized carbon groups;[47] similar chromophores may also exist on the hydrogenated graphenes.[8,14] The emission intensities for both H-SLG and H-BLG are nonuniform across the sheets, being strongest at the H-SLG and H-BLG edges (Figure 5c,d), consistent with these regions being the most reactive. It was also noted that the graphite flake exhibits the strongest fluorescence at its edges (Figure 5c). Finally, it is noted that

DOI: 10.1021/jacs.6b08625
J. Am. Chem. Soc. 2016, 138, 14980–14986

the centers of H-SLG flakes give rise to greater emission than those of H-BLG, in line with the extent of hydrogenation at the SLG interior being higher than that of BLG (Figure 5c,d).

CONCLUSION

Employing Li as the reductant and H_2O as the proton source, Birch-type reduction methodology was used to hydrogenate graphene, the extent of which has been quantified by Raman and X-ray photoelectron spectroscopies. Evolution of Raman maps as a function of reduction time revealed that FLG hydrogenation proceeds inward from defects or edges, a pathway often assumed but rarely investigated. Accessible defects/edges are not only the most reactive regions, but are also necessary. Indeed, pristine, gold-sealed FLG is inert toward the reagents employed, an observation that implicates an intercalation process. The hydrogenation of labeled $^{12}C/^{13}C$ bilayer and $^{12}C/^{13}C/^{12}C$ trilayer graphenes resulted in products whose individual sheets are comparably reduced, consistent with a reaction that proceeds from the graphene perimeter to the interior, and one in which the reagents must pass between graphene layers. The effects of Birch-type hydrogenation include strain, as revealed by bathochromically shifted Raman bands and surface deformation apparent in TEM and AFM images. Hydrogenation affects electronic band structure and leads to higher visible light transparency. Clear differences are also found in the fluorescence of H-SLG and H-BLG, with the latter exhibiting greater emission at its edges. In sum, our results describe the progress and products by subjecting well-defined carbon materials to a Birch-type reduction and are expected to facilitate the realization of ultrathin reduced motifs, including diamane, whose significance may grow beyond mere theoretical curiosity.

EXPERIMENTAL SECTION

Graphene Preparation. Kish or highly oriented pyrolytic graphite (HOPG) was mechanically exfoliated onto SiO_2 (300 nm)/Si using the Scotch-tape method.[48] CVD SLG was grown on Cu foil (Alfa Aesar, 25 μm) using natural abundance (98.9% $^{12}CH_4$) or $^{13}CH_4$ carbon sources. CVD graphene with FLG patches was grown by the pocket method.[49] Isotopically labeled graphene with FLG patches was grown using the pocket method, where the bilayer graphene was formed on the outside Cu surface as reported previously.[35,36] After Cu foil was annealed in vacuum at 1030 °C for 10 min, $^{13}CH_4$ at a flow rate of 5 sccm and hydrogen at a flow rate of 50 sccm were introduced for 30 min. Then, the $^{13}CH_4$ was turned off, and $^{12}CH_4$ turned on and flowed at 5 sccm for another 30 min. The as-prepared graphene was transferred onto SiO_2 (300 nm)/Si using PMMA as a protective layer.[50] The $^{12}C/^{13}C/^{12}C$ TLG was constructed from SLG samples.[51] Graphene employed in the TEM study was grown by CVD, and then transferred directly onto Quantifoil micromachined holey carbon TEM grids on 200 mesh Au. SLG and BLG samples used for XPS and UV−vis spectroscopy were, respectively, grown using CH_4 on Cu foil (Alfa Aesar, 25 μm, 99.8%) and Cu/Ni (90/10) foil (All Metal Sales, Inc., 100 μm, weight percent: 88.00% Cu, 9.90% Ni, 0.44% Mn, 1.54% Fe, and 0.10% Zn).[52] The as-prepared graphene was then transferred onto SiO_2 (300 nm)/Si for XPS or onto quartz for UV−vis characterization.

Birch-Type Reduction. Lithium (Honjo Metal Co., Ltd., >99.9%) foils were cut into small pieces under Ar. Deionized H_2O, CH_3OH (Sigma-Aldrich, anhydrous, 99.8%), and CH_3CH_2OH (Sigma-Aldrich, 99.8%) were used as H^+ donors. In a typical reaction, a 100 mL three-neck round-bottomed flask equipped with a dry ice condenser and a Dewar flask was flushed with Ar. Ammonia (~50 mL) was condensed into the flask at −78 °C, and the addition of lithium (105 mg, 15 mmol) afforded a blue solution that was stirred for 30 min. The supported graphene sample was immersed into the solution for the prescribed reduction time. A H^+ donor (5 mL) was added to the solution by syringe while keeping the sample inside, and the Dewar flask was removed. Unless otherwise mentioned, the graphene sample was taken out after the blue color of the solution disappeared (~2 min after H_2O addition). The sample was washed with several portions of CH_3OH and dried under a flow of N_2.

Thermal dehydrogenation was performed by placing hydrogenated graphene samples in a tube furnace under Ar (1.5×10^{-1} Torr) and ramping to the target temperature (300, 500, or 700 °C) over 30 min. The temperature was held constant for 3 h, after which the samples were cooled to room temperature and removed.

Characterization. AFM imaging was performed using a Bruker Nanoscope V ultralow current system. Measurements made use of the tapping mode to characterize surface morphology and the number of layers in the graphene samples. Raman data were acquired using two confocal microspectrometers (Alpha 300 R or Alpha 300 M+, WITec GmbH), each with a 532 nm laser source. Unless otherwise mentioned, a laser power of 1 mW was used to avoid sample damage. TEM images were acquired using a Cs image aberration-corrected FEI Titan (3) G2 60-300 with an electron monochromator set to 80 kV. In order to acquire DF-TEM images, the $\{10\bar{1}0\}$ spot diffracted from a hydrogenated graphene sheet was selected in a diffraction mode with an objective aperture diameter of 1.28 nm^{-1}. The acquisition time for DF-TEM was 3 s per frame. EELS data were recorded using a Gatan GIF Quantum 965 electron energy loss spectrometer. XPS data were acquired with a Thermo Fisher K-Alpha spectrometer system. UV−vis spectra were recorded using an Agilent Cary 100 UV−vis spectrometer. Fluorescence spectra were obtained in the backscattered geometry with a 40× objective lens (numerical aperture is 0.60) on a home-built Raman spectrometer,[34] with a diode-pumped solid-state laser (λ = 457.0 nm) as the excitation source. The spectral width of the Rayleigh scattering peak was 0.3 nm, and spectral precision was ~0.1 nm. The average power of the excitation laser beam was 0.1 mW, and the laser was focused into a spot of diameter ~1 μm. The backscattered signal was fed into a spectrograph (focal length 300 nm) equipped with a N_2-cooled CCD detector. Two-dimensional fluorescence maps were obtained every 1 μm using an $x-y$ motorized stage.

ASSOCIATED CONTENT

Supporting Information

The Supporting Information is available free of charge on the ACS Publications website at DOI: 10.1021/jacs.6b08625.

Additional characterization information and supporting references and notes (PDF)

AUTHOR INFORMATION

Corresponding Author

*ruofflab@gmail.com

Notes

The authors declare no competing financial interest.

ACKNOWLEDGMENTS

This work was supported by IBS-R019-D1. S.C. acknowledges the financial support from the National Natural Science Foundation (Grants 51302233 and 11374244) of China. Z.L. was also supported by the National Research Foundation of Korea (NRF) grant funded by the Korea government (MSIP) (No. 2015R1A2A2A01006992). S.R. was supported by the Center for Advanced Soft-Electronics funded by the Ministry of Science, ICT and Future Planning of Korea as Global Frontier Project (NRF-2011-0031630). X.Z. thanks S. H. Lee, X. Chen, M. Saxena, and D. Luo for assistance with characterization of these materials. C.W.B. acknowledges the BK21 Plus Program as funded by the Ministry of Education and the National Research Foundation of Korea.

DOI: 10.1021/jacs.6b08625
J. Am. Chem. Soc. 2016, 138, 14980−14986

REFERENCES

(1) Sofo, J. O.; Chaudhari, A. S.; Barber, G. D. *Phys. Rev. B: Condens. Matter Mater. Phys.* **2007**, *75*, 153401.
(2) Boukhvalov, D. W.; Katsnelson, M. I.; Lichtenstein, A. I. *Phys. Rev. B: Condens. Matter Mater. Phys.* **2008**, *77*, 035427.
(3) Zhou, J.; Wang, Q.; Sun, Q.; Chen, X. S.; Kawazoe, Y.; Jena, P. *Nano Lett.* **2009**, *9*, 3867−3870.
(4) Pumera, M.; Wong, C. H. A. *Chem. Soc. Rev.* **2013**, *42*, 5987−5995.
(5) Elias, D. C.; Nair, R. R.; Mohiuddin, T. M. G.; Morozov, S. V.; Blake, P.; Halsall, M. P.; Ferrari, A. C.; Boukhvalov, D. W.; Katsnelson, M. I.; Geim, A. K.; Novoselov, K. S. *Science* **2009**, *323*, 610−613.
(6) Balog, R.; Jorgensen, B.; Nilsson, L.; Andersen, M.; Rienks, E.; Bianchi, M.; Fanetti, M.; Laegsgaard, E.; Baraldi, A.; Lizzit, S.; Sljivancanin, Z.; Besenbacher, F.; Hammer, B.; Pedersen, T. G.; Hofmann, P.; Hornekaer, L. *Nat. Mater.* **2010**, *9*, 315−319.
(7) Luo, Z. Q.; Shang, J. Z.; Lim, S. H.; Li, D. H.; Xiong, Q. H.; Shen, Z. X.; Lin, J. Y.; Yu, T. *Appl. Phys. Lett.* **2010**, *97*, 233111.
(8) Schafer, R. A.; Englert, J. M.; Wehrfritz, P.; Bauer, W.; Hauke, F.; Seyller, T.; Hirsch, A. *Angew. Chem., Int. Ed.* **2013**, *52*, 754−757.
(9) Sun, Z. Z.; Pint, C. L.; Marcano, D. C.; Zhang, C. G.; Yao, J.; Ruan, G. D.; Yan, Z.; Zhu, Y.; Hauge, R. H.; Tour, J. M. *Nat. Commun.* **2011**, *2*, 559.
(10) Ryu, S.; Han, M. Y.; Maultzsch, J.; Heinz, T. F.; Kim, P.; Steigerwald, M. L.; Brus, L. E. *Nano Lett.* **2008**, *8*, 4597−4602.
(11) Diankov, G.; Neumann, M.; Goldhaber-Gordon, D. *ACS Nano* **2013**, *7*, 1324−1332.
(12) Pekker, S.; Salvetat, J. P.; Jakab, E.; Bonard, J. M.; Forro, L. *J. Phys. Chem. B* **2001**, *105*, 7938−7943.
(13) Yang, Z. Q.; Sun, Y. Q.; Alemany, L. B.; Narayanan, T. N.; Billups, W. E. *J. Am. Chem. Soc.* **2012**, *134*, 18689−18694.
(14) Strauss, V.; Schäfer, R. A.; Hauke, F.; Hirsch, A.; Guldi, D. M. *J. Am. Chem. Soc.* **2015**, *137*, 13079−13086.
(15) Eng, A. Y. S.; Poh, H. L.; Sanek, F.; Marysko, M.; Matejkova, S.; Sofer, Z.; Pumera, M. *ACS Nano* **2013**, *7*, 5930−5939.
(16) Subrahmanyam, K. S.; Kumar, P.; Maitra, U.; Govindaraj, A.; Hembram, K. P. S. S.; Waghmare, U. V.; Rao, C. N. R. *Proc. Natl. Acad. Sci. U. S. A.* **2011**, *108*, 2674−2677.
(17) Whitener, K. E.; Lee, W. K.; Campbell, P. M.; Robinson, J. T.; Sheehan, P. E. *Carbon* **2014**, *72*, 348−353.
(18) Lee, W. K.; Whitener, K. E.; Robinson, J. T.; Sheehan, P. E. *Adv. Mater.* **2015**, *27*, 1774−1778.
(19) Eng, A. Y. S.; Sofer, Z.; Huber, S.; Bousa, D.; Marysko, M.; Pumera, M. *Chem. - Eur. J.* **2015**, *21*, 16828−16838.
(20) Zhang, Y. B.; Tang, T. T.; Girit, C.; Hao, Z.; Martin, M. C.; Zettl, A.; Crommie, M. F.; Shen, Y. R.; Wang, F. *Nature* **2009**, *459*, 820−823.
(21) Lee, J. H.; Avsar, A.; Jung, J.; Tan, J. Y.; Watanabe, K.; Taniguchi, T.; Natarajan, S.; Eda, G.; Adam, S.; Neto, A. H. C.; Ozyilmaz, B. *Nano Lett.* **2015**, *15*, 319−325.
(22) Rohrer, J.; Hyldgaard, P. *Phys. Rev. B: Condens. Matter Mater. Phys.* **2011**, *83*, 165423.
(23) Chernozatonskii, L. A.; Sorokin, P. B.; Kvashnin, A. G.; Kvashnin, D. G. *JETP Lett.* **2009**, *90*, 134−138.
(24) Odkhuu, D.; Shin, D.; Ruoff, R. S.; Park, N. *Sci. Rep.* **2013**, *3*, 3276.
(25) Rajasekaran, S.; Abild-Pedersen, F.; Ogasawara, H.; Nilsson, A.; Kaya, S. *Phys. Rev. Lett.* **2013**, *111*, 085503.
(26) Birch, A. J. *J. Chem. Soc.* **1944**, 430−436.
(27) Ferrari, A. C.; Meyer, J. C.; Scardaci, V.; Casiraghi, C.; Lazzeri, M.; Mauri, F.; Piscanec, S.; Jiang, D.; Novoselov, K. S.; Roth, S.; Geim, A. K. *Phys. Rev. Lett.* **2006**, *97*, 187401.
(28) Luo, Z. Q.; Yu, T.; Ni, Z. H.; Lim, S. H.; Hu, H. L.; Shang, J. Z.; Liu, L.; Shen, Z. X.; Lin, J. Y. *J. Phys. Chem. C* **2011**, *115*, 1422−1427.
(29) Ferreira, E. H. M.; Moutinho, M. V. O.; Stavale, F.; Lucchese, M. M.; Capaz, R. B.; Achete, C. A.; Jorio, A. *Phys. Rev. B: Condens. Matter Mater. Phys.* **2010**, *82*, 125429.
(30) Cancado, L. G.; Jorio, A.; Ferreira, E. H. M.; Stavale, F.; Achete, C. A.; Capaz, R. B.; Moutinho, M. V. O.; Lombardo, A.; Kulmala, T. S.; Ferrari, A. C. *Nano Lett.* **2011**, *11*, 3190−3196.
(31) Lucchese, M. M.; Stavale, F.; Ferreira, E. H. M.; Vilani, C.; Moutinho, M. V. O.; Capaz, R. B.; Achete, C. A.; Jorio, A. *Carbon* **2010**, *48*, 1592−1597.
(32) Ryu, S.; Liu, L.; Berciaud, S.; Yu, Y. J.; Liu, H. T.; Kim, P.; Flynn, G. W.; Brus, L. E. *Nano Lett.* **2010**, *10*, 4944−4951.
(33) Levesque, P. L.; Sabri, S. S.; Aguirre, C. M.; Guillemette, J.; Siaj, M.; Desjardins, P.; Szkopek, T.; Martel, R. *Nano Lett.* **2011**, *11*, 132−137.
(34) Lee, J. E.; Ahn, G.; Shim, J.; Lee, Y. S.; Ryu, S. *Nat. Commun.* **2012**, *3*, 1024.
(35) Hao, Y. F.; Wang, L.; Liu, Y. Y.; Chen, H.; Wang, X. H.; Tan, C.; Nie, S.; Suk, J. W.; Jiang, T. F.; Liang, T. F.; Xiao, J. F.; Ye, W. J.; Dean, C. R.; Yakobson, B. I.; McCarty, K. F.; Kim, P.; Hone, J.; Colombo, L.; Ruoff, R. S. *Nat. Nanotechnol.* **2016**, *11*, 426−431.
(36) Fang, W. J.; Hsu, A. L.; Song, Y.; Birdwell, A. G.; Amani, M.; Dubey, M.; Dresselhaus, M. S.; Palacios, T.; Kong, J. *ACS Nano* **2014**, *8*, 6491−6499.
(37) Cai, W. W.; Piner, R. D.; Stadermann, F. J.; Park, S.; Shaibat, M. A.; Ishii, Y.; Yang, D. X.; Velamakanni, A.; An, S. J.; Stoller, M.; An, J. H.; Chen, D. M.; Ruoff, R. S. *Science* **2008**, *321*, 1815−1817.
(38) Li, X. S.; Cai, W. W.; Colombo, L.; Ruoff, R. S. *Nano Lett.* **2009**, *9*, 4268−4272.
(39) Fang, W.; Hsu, A. L.; Caudillo, R.; Song, Y.; Birdwell, A. G.; Zakar, E.; Kalbac, M.; Dubey, M.; Palacios, T.; Dresselhaus, M. S.; Araujo, P. T.; Kong, J. *Nano Lett.* **2013**, *13*, 1541−1548.
(40) Hu, S.; Lozada-Hidalgo, M.; Wang, F. C.; Mishchenko, A.; Schedin, F.; Nair, R. R.; Hill, E. W.; Boukhvalov, D. W.; Katsnelson, M. I.; Dryfe, R. A. W.; Grigorieva, I. V.; Wu, H. A.; Geim, A. K. *Nature* **2014**, *516*, 227−230.
(41) Lee, J. H.; Tan, J. Y.; Toh, C. T.; Koenig, S. P.; Fedorov, V. E.; Neto, A. H. C.; Ozyilmaz, B. *Nano Lett.* **2014**, *14*, 2677−2680.
(42) Greenwood, J.; Phan, T. H.; Fujita, Y.; Li, Z.; Ivasenko, O.; Vanderlinden, W.; Van Gorp, H.; Frederickx, W.; Lu, G.; Tahara, K.; Tobe, Y.; Uji-i, H.; Mertens, S. F. L.; De Feyter, S. *ACS Nano* **2015**, *9*, 5520−5535.
(43) Mohiuddin, T. M. G.; Lombardo, A.; Nair, R. R.; Bonetti, A.; Savini, G.; Jalil, R.; Bonini, N.; Basko, D. M.; Galiotis, C.; Marzari, N.; Novoselov, K. S.; Geim, A. K.; Ferrari, A. C. *Phys. Rev. B: Condens. Matter Mater. Phys.* **2009**, *79*, 205433.
(44) Bangert, U.; Pan, C. T.; Nair, R. R.; Gass, M. H. *Appl. Phys. Lett.* **2010**, *97*, 253118.
(45) Li, Y. F.; Liu, S. L.; Datta, D.; Li, Z. H. *Sci. Rep.* **2015**, *5*, 16556.
(46) Bae, S.; Kim, H.; Lee, Y.; Xu, X. F.; Park, J. S.; Zheng, Y.; Balakrishnan, J.; Lei, T.; Kim, H. R.; Song, Y. I.; Kim, Y. J.; Kim, K. S.; Ozyilmaz, B.; Ahn, J. H.; Hong, B. H.; Iijima, S. *Nat. Nanotechnol.* **2010**, *5*, 574−578.
(47) Eda, G.; Lin, Y. Y.; Mattevi, C.; Yamaguchi, H.; Chen, H. A.; Chen, I. S.; Chen, C. W.; Chhowalla, M. *Adv. Mater.* **2010**, *22*, 505−509.
(48) Huang, Y.; Sutter, E.; Shi, N. N.; Zheng, J. B.; Yang, T. Z.; Englund, D.; Gao, H. J.; Sutter, P. *ACS Nano* **2015**, *9*, 10612−10620.
(49) Li, X. S.; Magnuson, C. W.; Venugopal, A.; Tromp, R. M.; Hannon, J. B.; Vogel, E. M.; Colombo, L.; Ruoff, R. S. *J. Am. Chem. Soc.* **2011**, *133*, 2816−2819.
(50) Li, X. S.; Cai, W. W.; An, J. H.; Kim, S.; Nah, J.; Yang, D. X.; Piner, R.; Velamakanni, A.; Jung, I.; Tutuc, E.; Banerjee, S. K.; Colombo, L.; Ruoff, R. S. *Science* **2009**, *324*, 1312−1314.
(51) Ji, H. X.; Zhao, X.; Qiao, Z. H.; Jung, J.; Zhu, Y. W.; Lu, Y. L.; Zhang, L. L.; MacDonald, A. H.; Ruoff, R. S. *Nat. Commun.* **2014**, *5*, 3317.
(52) Wu, Y. P.; Chou, H.; Ji, H. X.; Wu, Q. Z.; Chen, S. S.; Jiang, W.; Hao, Y. F.; Kang, J. Y.; Ren, Y. J.; Piner, R. D.; Ruoff, R. S. *ACS Nano* **2012**, *6*, 7731−7738.

DOI: 10.1021/jacs.6b08625
J. Am. Chem. Soc. 2016, 138, 14980−14986